Locally averaged thermal dissipation rate in turbulent thermal convection: A decomposition into contributions from different temperature gradient components

Xiaozhou He,[1] Emily S. C. Ching,[2] and Penger Tong[1,a)]
[1]*Department of Physics, Hong Kong University of Science and Technology, Clear Water Bay, Kowloon, Hong Kong*
[2]*Department of Physics and Institute of Theoretical Physics, The Chinese University of Hong Kong, Shatin, Hong Kong*

(Received 16 July 2010; accepted 20 January 2011; published online 28 February 2011)

Using a homemade local temperature gradient probe, the instantaneous thermal dissipation rate $\epsilon_T(\mathbf{r},t)$ is obtained in an aspect-ratio-one cylindrical convection cell filled with water. From the time series measurements, a locally averaged thermal dissipation $\epsilon_\tau(\mathbf{r},t)$ over a time interval τ is constructed. Herein we decompose $\epsilon_\tau(\mathbf{r},t)$ into three contributions $\epsilon_\tau^i(\mathbf{r},t)$ $(i=x,y,z)$ from the temperature gradient components in the x, y, and z directions and systematically study their statistics and scaling properties. It is found that the moments of $\epsilon_\tau^i(\mathbf{r},t)$ exhibit good scaling in τ, i.e., $\langle(\epsilon_\tau^i)^p\rangle \sim \tau^{\mu^i(p)}$, for all three components and for p up to 6. The obtained exponents $\mu^i(p)$ at three representative locations in the convection cell are explained by a phenomenological model, which combines the effects of velocity statistics and geometric shape of the most dissipative structures in turbulent convection. © *2011 American Institute of Physics*. [doi:10.1063/1.3555637]

I. INTRODUCTION

Fluid turbulence as a nonequilibrium process is characterized by its unique structure and dynamics of the dissipation fields. The properties of the dissipation field determine not only the global transport of turbulence but also the statistics of local fluctuations. In turbulent Rayleigh–Bénard convection, where a fluid layer of thickness H is heated from below and cooled from the top, there are two dissipation fields associated with the convective flow. One is the viscous dissipation rate

$$\epsilon_u(\mathbf{r},t) = \frac{1}{2}\nu\sum_{ij}[\partial_i u_j(\mathbf{r},t) + \partial_j u_i(\mathbf{r},t)]^2, \tag{1}$$

where ν is the kinematic viscosity and $\partial_i u_j + \partial_j u_i$ is the symmetric part of the velocity gradient tensor field. The other is the thermal dissipation rate

$$\epsilon_T(\mathbf{r},t) = \kappa|\nabla T(\mathbf{r},t)|^2, \tag{2}$$

where κ is the thermal diffusivity and $\nabla T(\mathbf{r},t)$ is the temperature gradient field. The dissipation rates are always positive and the determination of $\epsilon_u(\mathbf{r},t)$ involves simultaneous measurements of the nine components of the velocity gradient tensor $\partial_i u_j(\mathbf{r},t)$. Temperature is a scalar and the determination of $\epsilon_T(\mathbf{r},t)$ only involves simultaneous measurements of the three components of the temperature gradient vector $\nabla T(\mathbf{r},t)$.

In thermal convection, the global average of $\epsilon_u(\mathbf{r},t)$ and $\epsilon_T(\mathbf{r},t)$ is directly linked to the total heat flux transported vertically through the convection cell. In particular, one finds[1]

$$\epsilon_T \equiv \langle\epsilon_T(\mathbf{r},t)\rangle_{V,t} = \kappa(\Delta T/H)^2 \mathrm{Nu(Ra,\ Pr)}, \tag{3}$$

where ΔT is the temperature difference across the convection cell of height H, Nu(Ra, Pr) is the Nusselt number (normalized heat flux), and $\langle\ldots\rangle_{V,t}$ represents averages over the fluid volume V and time t. The Nusselt number Nu(Ra, Pr) depends on two experimental control parameters. One is the Rayleigh number $\mathrm{Ra}=\alpha g\Delta T H^3/(\nu\kappa)$, where g is the gravitational acceleration, and α is the thermal expansion coefficient of the convecting fluid. The other control parameter is the Prandtl number $\mathrm{Pr}=\nu/\kappa$.

The theory of Grossmann and Lohse[2,3] explains the scaling behavior of Nu(Ra, Pr) by a decomposition of the mean thermal dissipation ϵ_T into the boundary layer and bulk contributions, which have different scaling behavior with varying Ra and Pr. In a recent experiment, He *et al.*[4] carried out a systematic study of the spatial distribution of the thermal dissipation field in turbulent convection. A local temperature gradient probe consisting of four identical thermistors was made to directly measure $\epsilon_T(\mathbf{r},t)$ in a cylindrical convection cell filled with water. The measurements were conducted over varying Rayleigh numbers Ra and spatial positions $\mathbf{r}$ across the entire cell. It was found that $\epsilon_T(\mathbf{r}) \equiv \langle\epsilon_T(\mathbf{r},t)\rangle_t$ contains two contributions; one is generated by thermal plumes, present mainly in the plume-dominated bulk region, and decreases with increasing Ra. The other contribution comes from the mean temperature gradient, being concentrated in the upper and lower thermal boundary layers, and increases with Ra. The experiment revealed the important roles played by the thermal dissipation field in turbulent convection.

Besides the connection to the global heat transport, the viscous and thermal dissipation rates are also believed to play an important role in determining the statistics of local

a)Author to whom correspondence should be addressed. Electronic mail: penger@ust.hk.

velocity and temperature fluctuations. In the Kolmogorov 1941 theory (K41),[5] turbulence was considered as a cascade process, in which kinetic energy is transferred from large to small scales at a constant rate, which is given by the mean energy dissipation rate $\epsilon_u \equiv \langle \epsilon_u(\mathbf{r},t) \rangle_{V,t}$. K41 predicted that the velocity difference $\delta v(l)$ between two points separated by a distance l has universal statistics that depend only on l and ϵ_u, when l is within the inertial range. The measured scaling behavior of $\delta v(l)$, however, showed a large deviation from the K41 prediction.[6] A longstanding challenge in turbulence research is to understand the origin of this deviation, which is known as anomalous scaling. In 1962, Kolmogorov proposed the refined similarity hypothesis (K62),[7] which replaced the constant ϵ_u by a locally averaged energy dissipation rate $\epsilon_u(l)$ over a length l and attributed the origin of the anomalous scaling to the scale-dependence of the statistics of $\epsilon_u(l)$. Later, in 1974, Kraichnan[8] pointed out that the local energy dissipation rate is not an inertial-range quantity and proposed to replace it by the local energy transfer rate.

Similar problems of anomalous scaling also apply to a scalar field advected by a turbulent velocity field. In particular, the anomalous scaling of active scalars, such as temperature in turbulent thermal convection, remains elusive.[9] In analogy to the kinetic energy cascade, convective turbulence was also considered as a cascade process,[10] in which the variance of temperature fluctuations is transferred from large to small scales at a constant thermal dissipation rate, which is given by the mean thermal dissipation rate ϵ_T. An extension of K62 to turbulent convection leads to the proposal that a scale-dependent locally averaged thermal dissipation $\epsilon_T(l)$ would give rise to an anomalous scaling for the velocity and temperature increments.[11,12] Similarly, an extension of Kraichnan's proposal would lead to the statement that the origin of anomalous scaling is due to a scale-dependent transfer rate of the local temperature-variance. Indeed, the latter proposal was shown to be valid in a recent numerical study of the shell model for homogeneous turbulent convection.[13] In addition, by assuming that the locally averaged thermal dissipation rate over a time interval τ has a hierarchical structure of the She–Leveque form,[14] Ching and Kwok[15] made specific predictions for the scaling exponents of the moments of the locally averaged thermal dissipation rate.

A large amount of theoretical,[11,12,16–21] numerical,[22–26] and experimental[27–36] work has been devoted to the study of small-scale fluctuations in turbulent convection. Details about these studies have been reviewed recently by Lohse and Xia.[9] Most of the earlier measurements[27–36] focused on the power spectra and structure functions of local temperature and velocity fluctuations at a single point in space. Taylor's[37] frozen flow hypothesis was invoked either explicitly or implicitly to connect the time-domain results to the theoretical predictions made in the spatial domain. More recently, the space-resolved structure functions of velocity and temperature fluctuations were obtained in turbulent convection[38,39] using particle image velocimetry and multiple temperature probes. The space-resolved velocity and temperature structure functions measured at the cell center were reported[38] to show K41 behavior and the Obukhov–Corrsin (OC) scaling[40,41] for passive scalar at lower orders of moment p and deviations from K41 and the OC scaling were found at higher orders of p. The observed deviations (i.e., anomalous scaling) were found to be consistent with the hierarchy models of She and Leveque[14] for velocity in nonbuoyant flows and of Ruiz-Chavarria *et al.*[42] for passive scalars. On the other hand, evidence of the Bolgiano–Obukhov scaling[43,44] for temperature being an active scalar was reported[39] at scales close to the local Bolgiano length, which are larger than those investigated in Ref. 38. However, the interpretation of the experimental results are generally complicated by other effects in the convective flow, such as flow anisotropy and inhomogeneity, and the lack of spatial separation of the relevant length scales for the flow in a closed convection cell.[9]

To test the refined similarity ideas for anomalous scaling, one not only needs to check the scaling properties of the velocity and temperature structure functions, but also should examine the scale-dependent statistics of the dissipation fields in order to verify that the observed anomalous scaling in the velocity and temperature structure functions is indeed compatible with the scaling of the dissipation fields. In contrast with the large number of experimental studies of the velocity and temperature structure functions, direct measurements of the viscous and thermal dissipation rates in turbulent flows are rare.[9,45] This is partially due to the fact that simultaneous measurements of all the components of the velocity gradient tensor or the temperature gradient vector with adequate spatial and temporal resolutions are still challenging tasks.

In this paper, we report a systematic study of the scaling properties of the measured $\epsilon_T(\mathbf{r},t)$ in turbulent Rayleigh–Bénard convection. In a recent brief report,[46] we have shown that the moments of $\epsilon_\tau(\mathbf{r},t)$, which is a local average of the directly measured $\epsilon_T(\mathbf{r},t)$ over a time interval τ, exhibit good scaling in τ for all orders of moment up to order 6. In a separate experiment, Sun *et al.*[38] have shown that the scaling behavior of the measured temperature structure functions at the cell center is different from that near the sidewall. To address issues related to the flow anisotropy and inhomogeneity, herein we decompose the locally averaged thermal dissipation rate $\epsilon_\tau(\mathbf{r},t)$ into three terms, $\epsilon_\tau(\mathbf{r},t)=\Sigma_i \epsilon_\tau^i(\mathbf{r},t)$ $(i=x,y,z)$; each term results from a component of the temperature gradient vector in the corresponding direction. We focus our attention on the scaling properties of each contribution $\epsilon_\tau^i(\mathbf{r},t)$ at three representative locations in the cell: at the cell center far away from the boundaries, near the sidewall at midheight of the cell, and inside the thermal boundary layer close to the lower conducting plate. In the latter two locations, the flow field is inevitably influenced by the large-scale circulation that spans the height of the convection cell and by the thermal plumes erupted from the lower thermal boundary layer. Such a systematic study allows us to disentangle the intermittency effects from the flow anisotropy and inhomogeneity and thus to have a critical test on the theories of anomalous scaling.

The remainder of the paper is organized as follows. We first describe the theoretical model for the scaling exponent of moments of the local thermal dissipation rate in Sec. II.

The experimental apparatus and method are introduced in Sec. III. Experimental results are discussed in Sec. IV. Finally, the work is summarized in Sec. V.

II. THEORY

In the experiment to be described below, we used a small homemade temperature gradient probe consisting of four identical thermistors to measure the three components of the temperature gradient vector ∇T. The temperature gradient ∇T can be decomposed into a sum

$$\nabla T(\mathbf{r},t) = \nabla T_m(\mathbf{r}) + \nabla T_f(\mathbf{r},t), \tag{4}$$

where $T_m(\mathbf{r})$ is the mean temperature and $T_f(\mathbf{r},t)$ is the temperature fluctuation. Consequently, $\epsilon_T(\mathbf{r},t)$ contains three contributions

$$\epsilon_T(\mathbf{r},t) = \kappa[|\nabla T_m(\mathbf{r})|^2 + 2\nabla T_m(\mathbf{r})\cdot\nabla T_f(\mathbf{r},t) + |\nabla T_f(\mathbf{r},t)|^2]. \tag{5}$$

As discussed in Ref. 46, one can construct a locally averaged thermal dissipation rate $\epsilon_\tau(\mathbf{r},t)$ by averaging $\epsilon_T(\mathbf{r},t)$ over a time interval τ and we are interested in how the moments of $\epsilon_\tau(\mathbf{r},t)$ vary with τ. The mean gradient $\nabla T_m(\mathbf{r})$ is a time independent quantity and thus is not interesting. Because the mean value of $\nabla T_f(\mathbf{r},t)$ is zero, the τ-average of $\nabla T_f(\mathbf{r},t)$ will be very small. Therefore, the term $|\nabla T_f(\mathbf{r},t)|^2$ has the strongest time dependence and is denoted as

$$\epsilon_f(\mathbf{r},t) \equiv \kappa|\nabla T_f(\mathbf{r},t)|^2. \tag{6}$$

Furthermore, $\epsilon_f(\mathbf{r},t)$ contains three terms, $\epsilon_f^i(\mathbf{r},t)$ $(i=x,y,z)$; each is associated with a component of the temperature gradient, $\partial_i T_f(\mathbf{r},t)$, in the corresponding direction.

In this paper, we focus on the locally averaged contributions, $\epsilon_\tau^i(\mathbf{r},t)$ $(i=x,y,z)$, which is defined as

$$\epsilon_\tau^i(\mathbf{r},t) = \frac{1}{\tau}\int_t^{t+\tau} \kappa[\partial_i T_f(\mathbf{r},t')]^2 dt', \tag{7}$$

and study the τ-dependence of the moments $\langle(\epsilon_\tau^i)^p\rangle \equiv \langle[\epsilon_\tau^i(\mathbf{r},t)]^p\rangle_t$, averaged over time t at three representative positions in the convection cell. The basic theoretical framework for the scaling behavior of the individual moments $\langle(\epsilon_\tau^i)^p\rangle$ follows that for the total moments $\langle\epsilon_\tau^p\rangle$, as described in Ref. 46. Thus we only outline the key points below.

Assuming $\langle(\epsilon_\tau^i)^p\rangle$ has a hierarchical structure of the She–Leveque form,[14] one finds the following general solution:

$$\mu^i(p) = c(1-\beta^p) - \lambda p \tag{8}$$

for the scaling exponents $\mu^i(p)$ $(i=x,y,z)$, defined by

$$\langle(\epsilon_\tau^i)^p\rangle \sim \tau^{\mu^i(p)}. \tag{9}$$

In the above, c, $0<\beta<1$, and λ are parameters that have different physical meanings. As will be shown below, these parameters take different values along the x-, y-, and z-directions and at different positions. For $p=1$, one has

$$\langle\epsilon_\tau^i\rangle \approx \frac{1}{T_{\text{total}}}\int_0^{T_{\text{total}}} \kappa[\partial_i T_f(\mathbf{r},t')]^2 dt' \equiv \epsilon_0^i, \tag{10}$$

where T_{total} is the total time of measurement. Because ϵ_0^i is independent of τ, we have $\mu^i(1)=0$. As a result, the three parameters are related by

$$c(1-\beta) - \lambda = 0. \tag{11}$$

We now discuss the physical meaning of the three parameters. First, from Eqs. (9) and (8), one finds

$$(\epsilon_\tau^i)^\infty = \lim_{p\to\infty}\left[\frac{\langle(\epsilon_\tau^i)^{p+1}\rangle}{\langle(\epsilon_\tau^i)^p\rangle}\right] \sim \tau^{-\lambda}. \tag{12}$$

As discussed in Ref. 46, $(\epsilon_\tau^i)^\infty$ can be dimensionally estimated as $\Delta T^2/t_r(\tau)$, where $t_r(\tau)\sim r/u_r$ is the eddy turn-over time at the scale $r\sim U\tau$, with U being a typical velocity in the flow. Depending on whether temperature is passive or active, the scaling behavior of u_r would be different. Specifically, when temperature is a passive scalar, the velocity fluctuations obey the K41 scaling[6] $u_r\sim(r\epsilon_u)^{1/3}$. In this case, we find $(\epsilon_\tau^i)^\infty\sim\tau^{-2/3}$, i.e., $\lambda=2/3$. On the other hand, in the buoyancy-dominated region where temperature is an active scalar, the velocity fluctuations obey the Bolgiano–Obukhov scaling: $u_r\sim(\alpha g)^{2/5}(\epsilon_T)^{-1/5}r^{3/5}$. In this case, we find $(\epsilon_\tau^i)^\infty\sim\tau^{-2/5}$, i.e., $\lambda=2/5$.

In short, the value of λ depends on the scaling properties of velocity fluctuations in turbulent convection, which are, in turn, determined by whether temperature is active or passive. The parameter c is interpreted as the codimension of the most dissipative structures, i.e., the set of largest thermal dissipation rate. If the most dissipative structures are filamentlike $(D_\epsilon=1)$, one has $c=3-D_\epsilon=2$. Therefore, for passive scalars with sheetlike dissipative structures, we have $\lambda=2/3$, $c=1$, and $\beta=1/3$. On the other hand, for passive scalars with filamentlike dissipative structures, we have $\lambda=2/3$, $c=2$, and $\beta=2/3$. For active scalars with sheetlike dissipative structures, we have $\lambda=2/5$, $c=1$, and $\beta=3/5$. Finally, for active scalars with filamentlike dissipative structures, we have $\lambda=2/5$, $c=2$, and $\beta=5/4$.

In the experiment to be described below, we will test the above phenomenological theory for the individual moments $\langle(\epsilon_\tau^i)^p\rangle$ $(i=x,y,z)$. In particular, the phenomenological theory made three important predictions, which can be checked directly with the experimental data: (i) The scaling exponents $\mu^i(p)$ are given in Eq. (8) in terms of two independent parameters c and λ. (ii) The parameter λ takes two distinct values $\lambda_{\text{active}}=2/5$ and $\lambda_{\text{passive}}=2/3$ depending on whether temperature is an active or passive scalar. (iii) The parameter c is the codimension of the sets of the largest thermal dissipation rates and takes a value of either 1 or 2, depending on whether the most dissipative structures are sheetlike or filamentlike. It is expected that the value of λ depends only on the height of the measuring position, whereas the value of c may change in the bulk and sidewall regions. These characteristic features of the convective flow based on the statistics of the thermal dissipation rate will be compared with those obtained from the temperature and velocity structure functions.

It should be pointed out that while the original hierarchical model of She and Leveque[14] was proposed for local energy dissipation rates, averaged over a spatial region, we are here working with the local thermal dissipative rates, averaged over a time interval. As a result, our scaling results can be tested directly using the time series data available in the experiment. In particular, Taylor's frozen flow hypothesis[37] is not used in the derivations. To link the scaling exponents $\mu^i(p)$ with those of the temperature and velocity structure functions, some kind of refined similarity ideas have to be used.

III. EXPERIMENT

The experiment is conducted in a upright cylindrical convection cell filled with water. The inner diameter of the cell is $D=19.0$ cm and its height $H=20.5$ cm. The corresponding aspect ratio of the cell is $\Gamma=D/H\simeq 1$. Details about the apparatus and experimental method have been described elsewhere[4] and here we mention only some key points. The sidewall of the cell is made of a transparent Plexiglas ring with a wall thickness of 0.6 cm. The top and bottom plates are made of ~1 cm thick brass plates and their surfaces are electroplated with a thin layer of gold. The Plexiglas ring is sandwiched between the two plates and is sealed to the top and bottom plates via two rubber O rings. Two silicon rubber film heaters connected in parallel are sandwiched on the backside of the bottom plate to provide constant and uniform heating. The upper side of the top plate together with a circular aluminum cover form a closed cooling chamber, whose temperature is maintained constant by circulating cold water from a temperature controlled bath. The temperature difference ΔT between the top and bottom plates is measured by two thermistors embedded in each plate. In the experiment, the value of ΔT varies from 4.8 to 50 °C depending on the heating power. By adjusting the temperature of the cooling water, we maintain the temperature of the bulk fluid at ~30 °C for all the measurements. At this temperature, one has $\nu\simeq 8.2\times 10^{-3}$ cm^2/s, $\kappa\simeq 1.5\times 10^{-3}$ cm^2/s, and the corresponding Prandtl number $\mathrm{Pr}=\nu/\kappa\simeq 5.5$. The temperature stability of the top and bottom plates is found to be within 0.1 °C in standard deviation, which is less than 2% of the minimum ΔT used in the experiment. The entire convection cell is placed inside a square thermostat box, whose temperature matches the mean temperature of the bulk fluid to prevent heat exchange between the convecting fluid (water) and the surroundings.

The temperature gradient probe is made of four small thermistor beads of 0.11 mm in diameter (BB05JA243N, GE Thermometrics) and is assembled in our own laboratory. Each of them has a semiconductor head of 80 μm in diameter and two 1-cm-long metal legs of 10 μm in diameter. Silver paste is used to glue each of the metal legs to a 100-μm-diameter copper extension wire. The thermistor assembly is then coated with a thin layer of waterproof varnish for use in water. The four identical thermistors are used to measure the three components of the local temperature gradient simultaneously. One of the thermistors is placed at the origin, labeled as T_0, and the other three thermistors are arranged along the x-, y-, and z-axes, respectively. By simultaneously measuring the four temperature signals, we obtain the three temperature gradient components $\delta T_i/\delta\ell$, where $\delta T_i=T_i-T_0$ $(i=x,y,z)$ is the temperature difference between a pair of the thermistors with separation $\delta\ell=0.25\pm 0.1$ mm. All the thermistors are calibrated individually with an accuracy of ~5 mK for δT_i. Each of the thermistors is connected to an ac transformer bridge as a resistor arm and the bridge is driven by a lock-in amplifier at a working frequency $f_0\simeq 1\pm 0.2$ kHz. Four identical bridges and lock-in amplifiers are used and the sampling rate of the temperature measurements is set at 40 Hz. Typically, we take (12–30)-h-long time series data [corresponding to $(1.7–4.3)\times 10^6$ data points] at a fixed location in the cell. All measurements reported here are conducted in the rotation plane of the large-scale circulation.

To accurately measure the local gradient of the temperature field, one needs to keep the separation $\delta\ell$ between the thermistors as small as possible. This separation should be smaller than the thermal boundary layer thickness δ, which is the smallest dissipation length in turbulent thermal convection. At length scales smaller than δ, temperature fluctuations are dissipated by diffusion. On the other hand, the probe separation should be large enough to minimize the disturbances produced by a thermistor tip to the nearby temperature measurements. In the experiment, we chose the thermistor's separation at a minimal value of $\delta\ell=0.25\pm 0.1$ mm, which is 2.3 times larger than the tip diameter of the thermistor but 3.2 times smaller than the measured value of δ at $\mathrm{Ra}=3.6\times 10^9$ (≃0.8 mm). In a previous experiment,[4] we have thoroughly tested the temperature gradient probe. It was found that the temperature histograms and power spectra measured by the four thermistors superpose nicely with each other, indicating that the temperature signal measured by one of the thermistors is not affected by the surrounding ones, at least in the statistical sense. Since the time constant of the thermistors is smaller than 15 ms, the temporal resolution of the temperature time series measurements is determined by the sampling time, which is 25 ms. As will be shown in Sec. IV A, this temporal resolution is adequate to resolve temperature fluctuations corresponding to ten Kolmogorov viscous lengths.

IV. RESULTS AND DISCUSSION

The recent temperature, velocity, and flow visualization measurements[47–49] have revealed that the spatial distribution of thermal plumes, which drive the convective flow in a closed cell, is neither homogeneous nor isotropic. The thermal plumes organize themselves in such a way that warm plumes accumulate on one side of the cell and cold plumes concentrate on the opposite side of the cell. The spatially separated warm and cold plumes exert buoyancy forces on the fluid and drive the vertical flow near the sidewall. The central bulk region of the flow is approximately homogeneous and is "sheared" by the rising and falling plumes, resulting in a large-scale circulation (LSC) across the cell height. This large-scale circulation provides a fast channel along the cell periphery for the transport of heat.[50]

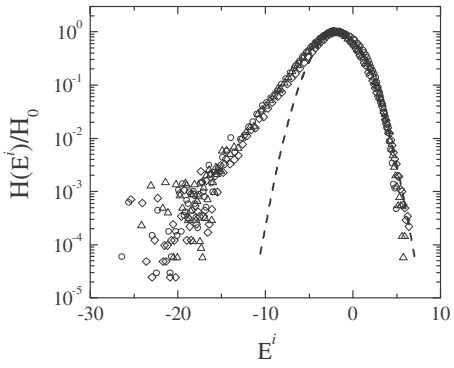

FIG. 1. Measured histograms $H(E^x)/H_0$ (circles), $H(E^y)/H_0$ (triangles), and $H(E^z)/H_0$ (diamonds) for the three contributions of the local thermal dissipation rate at the cell center with $\mathrm{Ra}=8.3\times10^9$. The dashed line shows a Gaussian function $H(E^i)/H_0=\exp\{-(E^i-m)^2/2\sigma^2\}$, with $m=-1.8$ and $\sigma=2$ (see text).

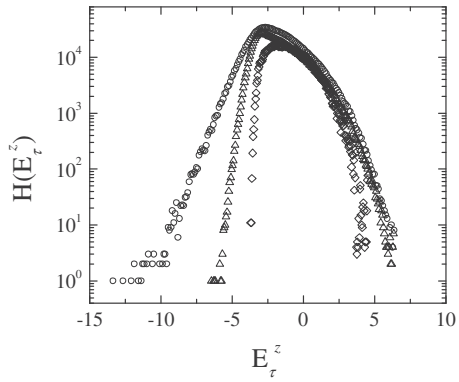

FIG. 2. Measured histograms $H(E_\tau^z)$ as a function of E_τ^z for three different values of τ: 0.075 (circles), 0.25 (triangles), and 5 s (diamonds). The measurements are made at the cell center with $\mathrm{Ra}=8.3\times10^9$.

With this understanding of plume dynamics, we now discuss the scaling behavior of $\epsilon_\tau(\mathbf{r},t)$ at three representative locations in the convection cell: at the cell center (12.4-h-long time series data), near the sidewall (at the middle height of the cell and 1 cm away from the cell wall; 14.8-h-long time series data), and near the lower conducting plate (above the center of the bottom plate; three sets of data of various durations). All locations are in the rotation plane of LSC. To take the flow anisotropy into account, we first examine the statistics of the dissipation components $\epsilon_\tau^i(\mathbf{r},t)$ $(i=x,y,z)$ and then study the total dissipation rate $\epsilon_\tau(\mathbf{r},t)=\Sigma_i\epsilon_\tau^i(\mathbf{r},t)$. It is found that the scaling of $\epsilon_\tau^i(\mathbf{r},t)$ $(i=x,y,z)$ [and $\epsilon_\tau(\mathbf{r},t)$] remains the same in the Ra range studied $(9\times10^8\le\mathrm{Ra}\le9\times10^9)$. Hereafter, we focus on the results at fixed values of Ra.

A. At the cell center

Figure 1 shows the measured histograms $H(E^x)/H_0$ (circles), $H(E^y)/H_0$ (triangles), and $H(E^z)/H_0$ (diamonds) for the three contributions of the local thermal dissipation rate at the cell center with $\mathrm{Ra}=8.3\times10^9$. In the plot, the histograms are normalized by their maximum value H_0 and the dissipation variables ϵ_f^i $(i=x,y,z)$ are expressed as $E^i=\ln(\epsilon_f^i/\epsilon_0^i)$, where ϵ_0^i is the mean value of each component. Over an amplitude range of more than four decades, the measured $H(E^x)/H_0$, $H(E^y)/H_0$, and $H(E^z)/H_0$ overlap very well, suggesting that fluctuations of the local thermal dissipation rate at the cell center are approximately isotropic. It has been shown[4] that the measured histograms of the temperature gradient components dT/dx_i $(x_i=x,y,z)$ in the central region are all symmetric and have approximately the same shape.

Another feature shown in Fig. 1 is that the statistics of $\ln(\epsilon_f)$ (or E^i) are non-Gaussian, which is revealed by the visible asymmetry of the measured $H(E^i)$ for large values of $|E^i|(\gtrsim5)$. For comparison, we also plot in Fig. 1 a Gaussian function $H(E^i)/H_0=\exp\{-(E^i-m)^2/2\sigma^2\}$, with $m=-1.8$ and $\sigma=2$ (dashed line), which fits only part of the measured $H(E^i)$ curve for $E^i\gtrsim-5$. Figure 1 thus demonstrates that the probability density function of ϵ_f^i is not logarithmic-Gaussian or logarithmic-normal, which were proposed to describe the intermittent nature of fluctuations of the viscous and thermal dissipations.[51–53] In a recent numerical study,[54] Emran and Schumacher also studied the non-Gaussian behavior of thermal dissipation fluctuations.

Figure 2 shows the measured histograms $H(E_\tau^z)$ as a function of E_τ^z for three different values of the averaging time τ: 0.075 (circles), 0.25 (triangles), and 5 s (diamonds). Here the horizontal variable is defined as $E_\tau^z=\ln(\epsilon_\tau^z/\epsilon_0^z)$, where ϵ_0^z is the mean vale of ϵ_τ^z. The shape of the obtained $H(E_\tau^z)$ changes continuously with increasing τ; the distribution width of $H(E_\tau^z)$ becomes narrower as τ increases. By comparing the time series data of $\epsilon_\tau^z(\mathbf{r},t)$ and $\epsilon_f^z(\mathbf{r},t)$, we find that the main effect of the time averaging is to smear out small-amplitude fluctuations in $\epsilon_f^z(\mathbf{r},t)$, as evidenced by the large change in the negative tail part of $H(E_\tau^z)$. The time averaging causes the narrowing of the distribution width, but the mean value of $\epsilon_\tau^z(\mathbf{r},t)$ does not change with τ and remains the same as that of $\epsilon_f^z(\mathbf{r},t)$.

Figure 3(a) shows the normalized z-moments $\langle(\epsilon_\tau^z)^p\rangle/(\epsilon_0^z)^p$ as a function of τ for $p=2$, 4, and 6 (from bottom to top). For $p=1$, we have $\langle(\epsilon_\tau^z)^1\rangle=\epsilon_0^z$ and thus $\mu^z(1)=0$. This is indeed observed. For $p>1$, the measured $\langle(\epsilon_\tau^z)^p\rangle/(\epsilon_0^z)^p$ decrease with τ until they reach to unity at large values of τ. Such a convergence at large values of τ is required and adequate statistics are needed in order to reach the asymptotic value. The measured $\langle(\epsilon_\tau^z)^p\rangle/(\epsilon_0^z)^p$ saturate at small values of τ, indicating that the sampling rate used for the temperature gradient measurements is adequate to catch all the fluctuations. As indicated by the solid lines in Fig. 3(a), a good power-law regime is found for all $\langle(\epsilon_\tau^z)^p\rangle/(\epsilon_0^z)^p$ with p up to 6. The scaling range in τ is about a decade long, ranging from 1 to 21 s.

The turnover time τ_0 of the large-scale circulation was found to be of the same order as the period of the velocity and temperature oscillations observed in the system[55,56] and one has $\tau_0\simeq35$ s at $\mathrm{Ra}\simeq8.3\times10^9$.[55] Besides the system size H, there are two more characteristic lengths (and times) in turbulent convection. The Bolgiano scale L_B, above which buoyancy becomes significant, was first defined[45] using the mean energy dissipation rate ϵ_u and thermal dissipation rate ϵ_T that are averaged over the entire convection cell: $L_B=(\alpha g)^{-3/2}(\epsilon_u)^{5/4}(\epsilon_T)^{-3/4}$. Because the energy and thermal

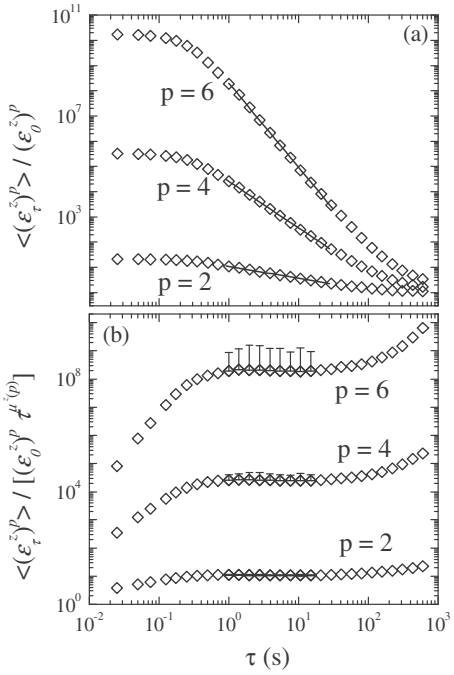

FIG. 3. (a) Normalized vertical moments $\langle(\epsilon_\tau^z)^p\rangle/(\epsilon_0^z)^p$ as a function of τ for $p=2$, 4, and 6 (from bottom to top). The solid lines indicate the power-law region. (b) Compensated plot $\langle(\epsilon_\tau^z)^p\rangle/[(\epsilon_0^z)^p\tau^{\mu^z(p)}]$ as a function of τ for $p=2$, 4, and 6 (from bottom to top) using the same data set as shown in (a). All the measurements are made at the cell center with $\mathrm{Ra}=8.3\times10^9$.

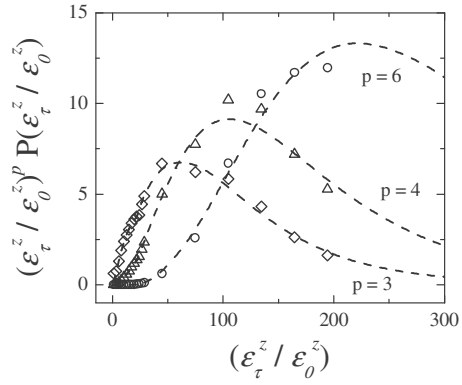

FIG. 4. Obtained kernel functions $(\epsilon_\tau^z)^pP(\epsilon_\tau^z)$ for $p=3$ (diamonds), 4 (triangles), and 6 (circles). In the plot, ϵ_τ^z is normalized by its mean value ϵ_0^z and the smallest time in the scaling range ($\tau=1$ s) is used. The dashed lines indicate the kernel functions obtained by using Eq. (13) with $P_0=0.0578$, $c=1.201$, and $d=0.489$. To plot all the curves in the same graph, the vertical scales for $p=4$ and $p=6$ have been reduced by a factor of 40 and 2×10^5, respectively.

dissipation rates vary with the height z relative to the bottom surface of the cell, one needs to consider a local Bolgiano scale[57] $L_B(z)=(\alpha g)^{-3/2}[\epsilon_u(z)]^{5/4}[\epsilon_T(z)]^{-3/4}$, where $\epsilon_u(z)$ and $\epsilon_T(z)$ are, respectively, the energy and thermal dissipation rates averaged over the cross section of the cell. In a numerical simulation at moderate Ra,[23] it was found that $L_B(H/2)/H\simeq0.88$ at the cell center. Associating τ_0 with H, we define the local Bolgiano time $\tau_B(z)\simeq\tau_0L_B(z)/H$ and find that $\tau_B(H/2)$ ($\simeq31$ s) is comparable to τ_0 at the cell center. The Kolmogorov viscous length $\eta\equiv(\nu^3/\epsilon_u)^{1/4}$ is a shorter length and is given by[1,31] $\eta/H=\mathrm{Pr}^{1/2}[\mathrm{Ra}(\mathrm{Nu}-1)]^{1/4}$. Using the measured Nu(Ra) in a similar convection cell,[58] we find $\eta/H\simeq2.3\times10^{-3}$ at $\mathrm{Ra}=8\times10^9$. If one takes the dissipative length to be 10η, the corresponding dissipative time $\tau_d\simeq\tau_0(10\eta)/H$ will be 0.8 s. Thus, at the cell center, the scaling range starts from τ_d and ends before $\tau_B(H/2)\simeq\tau_0$. A similar scaling range in τ was also found for the temperature structure functions, $S_p(\tau)\equiv\langle|\delta T_\tau|^p\rangle$.[34,59]

To display the power-law scaling more clearly, we show in Fig. 3(b) the compensated plot $\langle(\epsilon_\tau^z)^p\rangle/[(\epsilon_0^z)^p\tau^{\mu^z(p)}]$ as a function of τ for $p=2$, 4, and 6 (from bottom to top) using the same data set as shown in Fig. 3(a). The flat part of $\langle(\epsilon_\tau^z)^p\rangle/[(\epsilon_0^z)^p\tau^{\mu^z(p)}]$ reveals the scaling in τ. For a common scaling range in τ (which is chosen from the $p=6$ curve), we use the least-square method to fit all the data and find the exponent, $\mu^z(p)$, for all values of p up to 6. In contrast with the nice scaling behavior of $\langle(\epsilon_\tau^z)^p\rangle$, no discernible scaling was observed for the temperature structure functions, when $S_p(\tau)$ is plotted directly against τ on log-log scales.[35,59] Instead, the extended self-similarity method[21] was used to describe the scaling behavior of $S_p(\tau)$.

To check the accuracy of the obtained $\mu^z(p)$, we examine the convergence level of the kernel function $(\epsilon_\tau^z)^pP(\epsilon_\tau^z)$, where $P(\epsilon_\tau^z)$ is the probability density function of ϵ_τ^z. Figure 4 shows the obtained $(\epsilon_\tau^z)^pP(\epsilon_\tau^z)$ for $p=3$ (diamonds), 4 (triangles), and 6 (circles). In the plot, the dissipation variable ϵ_τ^z is normalized by its mean value ϵ_0^z and the smallest time in the scaling range ($\tau=1$ s) is used. It is seen that the kernel function $(\epsilon_\tau^z)^pP(\epsilon_\tau^z)$ converges well for small values of p ($p\lesssim3$). The convergence level of $(\epsilon_\tau^z)^pP(\epsilon_\tau^z)$ becomes weaker with increasing values of p. Note that because ϵ_τ^z goes as δT^2, the moment of ϵ_τ^z of order p corresponds to the temperature structure function of order $2p$. The dashed lines in Fig. 4 show the kernel functions obtained by using a fitted (analytical) function for $P(\epsilon_\tau^z)$. It has been shown[60] that the measured $P(\epsilon_\tau^z)$ can be well described by a stretched exponential function

$$P(\epsilon_\tau^z)=P_0\exp[-c(\epsilon_\tau^z/\sigma_z)^d], \tag{13}$$

where P_0 is the normalization factor and c and d are two fitting parameters which vary with τ slightly. Using the dashed lines, one can perform numerical integration over the kernel functions for different values of τ and p and find the differences in $\langle(\epsilon_\tau^z)^p\rangle/(\epsilon_0^z)^p$ between the estimated values by using Eq. (13) and those obtained directly from the data. These differences set the error bar size as shown in Fig. 3(b).

To further verify the scaling behavior of $\langle(\epsilon_\tau^z)^p\rangle/(\epsilon_0^z)^p$, we use the extended self-similarity (ESS) method[21] to analyze the thermal dissipation data. With ESS, we plot all the moments $\langle(\epsilon_\tau^z)^p\rangle/(\epsilon_0^z)^p$ against the normalized third moment $\langle(\epsilon_\tau^z)^3\rangle/(\epsilon_0^z)^3$ on log-log scales; an example is shown in Fig. 5. Indeed, the scaling range of $\langle(\epsilon_\tau^z)^p\rangle/(\epsilon_0^z)^p$ is extended to the entire data range considered here (solid lines). The same scaling behavior is found for all three dissipation components $\epsilon_\tau^i(\mathbf{r},t)$ $(i=x,y,z)$ at three different positions in the cell.

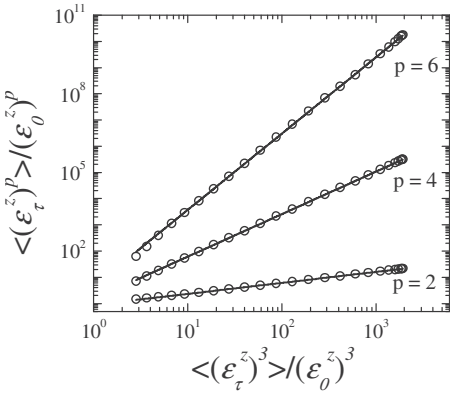

FIG. 5. ESS plots of the normalized vertical moments $\langle(\epsilon_\tau^z)^p\rangle/(\epsilon_0^z)^p$ as a function of $\langle(\epsilon_\tau^z)^3\rangle/(\epsilon_0^z)^3$ for $p=2$, 4, and 6 (from bottom to top) using the same data set as shown in Fig. 3. The solid lines indicate the power-law region.

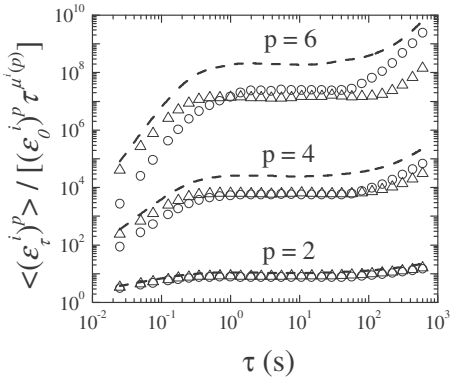

FIG. 7. Compensated plots $\langle(\epsilon_\tau^x)^p\rangle/[(\epsilon_0^x)^p\tau^{\mu^x(p)}]$ (circles) and $\langle(\epsilon_\tau^y)^p\rangle/[(\epsilon_0^y)^p\tau^{\mu^y(p)}]$ (triangles) as a function of τ for $p=2$, 4 and 6 (from bottom to top). The dashed lines indicate the corresponding compensated z-moments $\langle(\epsilon_\tau^z)^p\rangle/[(\epsilon_0^z)^p\tau^{\mu^z(p)}]$, shown in Fig. 3(b). All the measurements are made at the cell center with $\mathrm{Ra}=8.3\times10^9$.

In the following, we apply the same procedures and rigor to analyze the dissipation data and present only the essential scaling results below.

Figure 6 shows the obtained power-law exponents $\mu^z(p)$ as a function of p. The error bars in the plot indicate the fitting uncertainties found by fitting the data over the scaling range in τ between 1 and 21 s. Typical errors (peak to peak) for small p (=2) is ~10% and those for large p (=6) is ~35%. The values of $\mu^z(p)$ shown in Fig. 6 are all obtained from a time series data with 12.4 h duration time, which is about 1500 large-scale turnover times ($\tau_0\simeq30$ s), ensuring that the statistical averaging is adequate. It is seen that the values of $\mu^z(p)$ obtained from the compensated plots shown in Fig. 3(b) (circles) agree well with those obtained from the ESS plots shown in Fig. 5 (triangles).

The solid line in Fig. 6 is a plot of Eq. (8) with

$$c=1, \quad \lambda=\tfrac{2}{3}, \quad \beta=\tfrac{1}{3}. \quad \text{(central region)}. \tag{14}$$

The data can be adequately described by Eqs. (8) and (14) without any adjustable parameter. As discussed in Sec. II, the value $c=1$ suggests that the most dissipative structures at the cell center are two-dimensional and sheetlike. The value

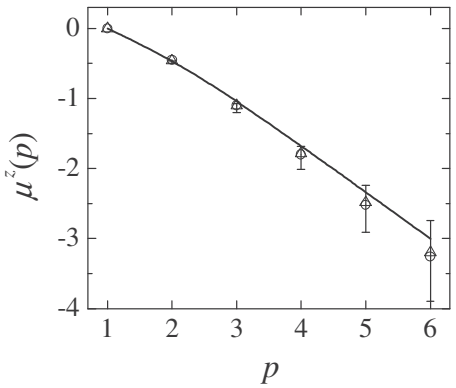

FIG. 6. Measured power-law exponents $\mu^z(p)$ as a function of p at the cell center with $\mathrm{Ra}=8.3\times10^9$. Circles are obtained from the compensated plots shown in Fig. 3(b) and triangles are obtained from the ESS plots shown in Fig. 5. The solid line is a plot of Eq. (8) with $c=1$, $\lambda=2/3$, and $\beta=1/3$ [Eq. (14)].

$\lambda=2/3$ indicates that the velocity fluctuations in the central region obey the K41 scaling[5,6] for nonbuoyant flows. This result thus suggests that in the central region, buoyancy effects are weak and do not affect the velocity statistics very much. In this sense, temperature behaves like a passive scalar. This conclusion agrees with those based on the measurement of temperature structure functions[31,38] and the numerical estimate that the local Bolgiano scale at the cell center is comparable to the cell height.[9,23]

In a similar manner, we also study the scaling behavior of the x- and y-moments $\langle(\epsilon_\tau^y)^p\rangle$ and $\langle(\epsilon_\tau^y)^p\rangle$ in the two horizontal directions perpendicular to gravity. Figure 7 shows the compensated plots $\langle(\epsilon_\tau^x)^p\rangle/[(\epsilon_0^x)^p\tau^{\mu^x(p)}]$ (circles) and $\langle(\epsilon_\tau^y)^p\rangle/[(\epsilon_0^y)^p\tau^{\mu^y(p)}]$ (triangles) as a function of τ for $p=2$, 4, and 6 (from bottom to top). Similar to the situation for $\langle(\epsilon_\tau^z)^p\rangle/[(\epsilon_0^z)^p\tau^{\mu^z(p)}]$, a common scaling (flat) region in τ is found for all the horizontal moments $\langle(\epsilon_\tau^i)^p\rangle/[(\epsilon_0^i)^p\tau^{\mu^i(p)}]$ $(i=x,y)$. Because of the symmetry of the convective flow, $\langle(\epsilon_\tau^x)^p\rangle/[(\epsilon_0^x)^p\tau^{\mu^x(p)}]$ and $\langle(\epsilon_\tau^y)^p\rangle/[(\epsilon_0^y)^p\tau^{\mu^y(p)}]$ are expected to be the same. Indeed, this is observed for p up to 6.

For comparison, we also include in Fig. 7 the compensated z-moments, $\langle(\epsilon_\tau^z)^p\rangle/[(\epsilon_0^z)^p\tau^{\mu^z(p)}]$, shown in Fig. 3(b) (dashed lines). For small values of p ($p\lesssim2$), the three compensated moments $\langle(\epsilon_\tau^i)^p\rangle/[(\epsilon_0^i)^p\tau^{\mu^i(p)}]$ $(i=x,y,z)$ are found to be approximately the same, indicating that the lower order statistics of dissipation fluctuations at the cell center are nearly isotropic. As the value of p increases, the difference between $\langle(\epsilon_\tau^z)^p\rangle/[(\epsilon_0^z)^p\tau^{\mu^z(p)}]$ and $\langle(\epsilon_\tau^i)^p\rangle/[(\epsilon_0^i)^p\tau^{\mu^i(p)}]$ $(i=x,y)$ becomes more pronounced. A recent study of the local convective heat flux in turbulent convection has shown[50] that while most thermal plumes are mixed up in the central region of the cell because of the strong velocity fluctuations in the region, there are still some unmixed warm and cold plumes left, which give rise to a nonzero local heat flux in the region. These remaining thermal plumes are also responsible for the generation of large but rare fluctuations of

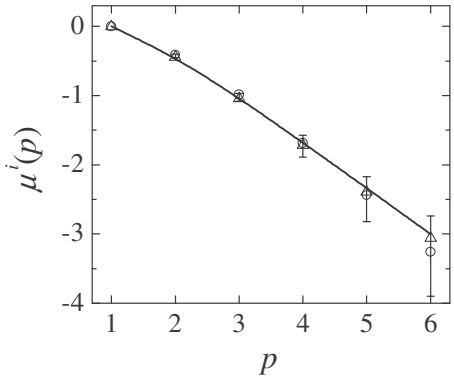

FIG. 8. Measured power-law exponents $\mu^x(p)$ (circles) and $\mu^y(p)$ (triangles) as a function of p at the cell center with $\mathrm{Ra}=8.3\times10^9$. Error bars are shown for circles. The solid line is a plot of Eq. (8) with $c=1$, $\lambda=2/3$, and $\beta=1/3$ [Eq. (14)].

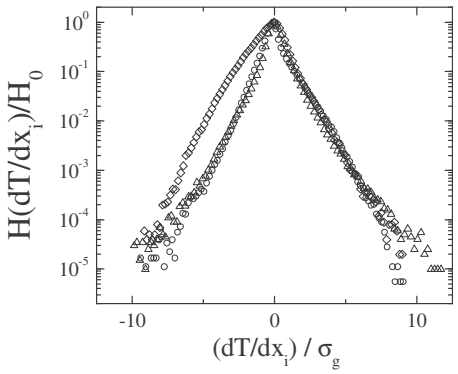

FIG. 10. Measured histograms $H(dT/dx)/H_0$ (circles), $H(dT/dy)/H_0$ (triangles), and $H(dT/dz)/H_0$ (diamonds) for the three components of the temperature gradient vector near the sidewall at $\mathrm{Ra}=8.3\times10^9$.

the local thermal dissipation rate,[4] which are more easily caught up by the higher order moments, $\langle(\epsilon_\tau^z)^p\rangle/(\epsilon_0^z)^p$ $(p\gtrsim4)$.

Figure 8 shows the measured power-law exponents $\mu^x(p)$ (circles) and $\mu^y(p)$ (triangles) as a function of p. The two sets of data overlap very well, indicating that the scaling exponents in the two horizontal directions are the same. Similar to the situation for $\mu^z(p)$, the obtained $\mu^x(p)$ and $\mu^y(p)$ both can be described by Eqs. (8) and (14) without any adjustable parameter (solid line). Figures 6 and 8 thus demonstrate that the scale-dependent statistics of the individual moments $\langle(\epsilon_\tau^i)^p\rangle$ $(i=x,y,z)$ at the cell center can be described by the same universal function.

Figure 9 shows how the exponent $\mu^z(p)$ varies with the spatial positions in the central region of the cell. The local thermal dissipation rate $\epsilon_\tau^z(\mathbf{r},t)$ is measured along the central axis of the cell and the obtained $\mu^z(p)$ versus p curves are plotted at different vertical distances z away from the center of the bottom plate: $z=100\delta$ (cell center, squares), 60δ (circles), 45δ (triangles), 25δ (crosses), and 11δ (diamonds).

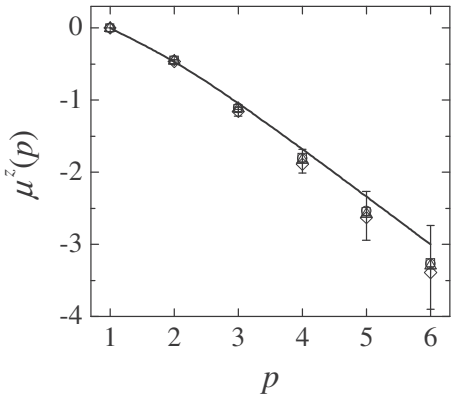

FIG. 9. Measured power-law exponents $\mu^z(p)$ as a function of p at different vertical positions along the central axis of the cell. The vertical distance z away from the center of the bottom plate $(z=0)$ is given as: $z=100\delta$ (cell center, squares), 60δ (circles), 45δ (triangles), 25δ (crosses), and 11δ (diamonds). Error bars are shown for squares. All the measurements are made at $\mathrm{Ra}=1.7\times10^9$ with $\delta\simeq0.99$ mm. The solid line is a plot of Eq. (8) with $c=1$, $\lambda=2/3$, and $\beta=1/3$ [Eq. (14)].

Here we take the z-axis pointing upward with the center of the bottom plate as its origin $(z=0)$. The values of z are expressed in units of the thermal boundary layer thickness δ, which has a value of $\delta\simeq0.99$ mm at $\mathrm{Ra}=1.7\times10^9$.[61] Except for a very small deviation at $z=11\delta$, all the data sets overlap very well and can be adequately described by Eqs. (8) and (14) without any adjustable parameter (solid line). Figure 9 thus reveals that the scaling exponent obtained at different locations in the central region remains the same. At $z=11\delta$, we find a very small but systematic decrease in the measured $\mu^z(p)$ for large values of p. It will be shown in Sec. IV C below, the measured $\mu^z(p)$ changes its scaling behavior when z is moved inside the thermal boundary layer.

B. Sidewall region at mid-height of the cell

Unlike the situation at the cell center, where velocity fluctuations are approximately isotropic with a zero mean, the velocity field near the sidewall is anisotropic with a dominant mean flow in the vertical direction.[47] Figure 10 shows the normalized histograms $H(dT/dx)/H_0$ (circles), $H(dT/dy)/H_0$ (triangles), and $H(dT/dz)/H_0$ (diamonds) for the three components of the temperature gradient vector near the sidewall. In the plot, the gradient variables dT/dx_i $(x_i=x,y,z)$ are normalized by their standard deviation σ_g. It is found that fluctuations of the two horizontal components are symmetric relative to the zero mean and their histograms overlap well over an amplitude range of more than five decades. The measured $H(dT/dz)/H_0$, however, shows a high level of asymmetry and is strongly skewed toward the negative derivatives. The negative skewness is caused by the fact that there are many warm plumes in the region and they lose heat while moving upward toward the top plate. In contrast, the measured $H(dT/dz)/H_0$ at the cell center has approximately the same shape as that of $H(dT/dx)/H_0$ and $H(dT/dy)/H_0$.[4]

Figure 11 shows the compensated plot of the moments $\langle(\epsilon_\tau^z)^p\rangle/[(\epsilon_0^z)^p\tau^{\mu^z(p)}]$ as a function of τ for $p=2$, 4, and 6 (from bottom to top). Similar to the situation at the cell center, a common scaling (flat) region in τ is found for all the values of p, suggesting that the vertical moment $\langle(\epsilon_\tau^z)^p\rangle/(\epsilon_0^z)^p$ has a good power-law scaling on τ. The scaling range in τ is be-

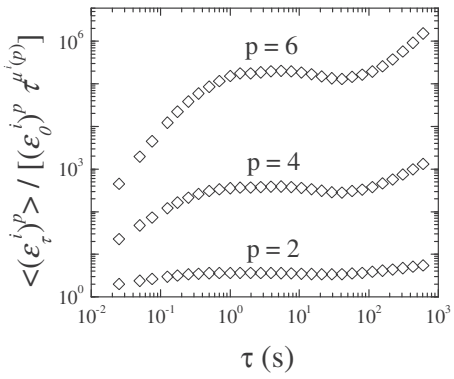

FIG. 11. Compensated plots $\langle(\epsilon_\tau^z)^p\rangle/[(\epsilon_0^z)^p \tau^{\mu^z(p)}]$ as a function of τ for $p=2$, 4, and 6 (from bottom to top). The measurements are made near the sidewall at $\mathrm{Ra}=8.3\times10^9$.

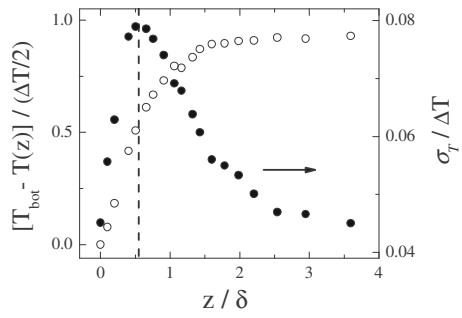

FIG. 13. Normalized mean temperature profile $[T_{\mathrm{bot}}-T(z)]/(\Delta T/2)$ (open circles) and rms temperature profile $\sigma_T(z)/\Delta T$ (solid circles) as a function of the normalized distance z/δ along the central axis of the cell. The measurements are made at $\mathrm{Ra}=1.75\times10^9$. The dashed line indicates the peak position of the measured $\sigma_T(z)/\Delta T$ at $z/\delta\simeq0.55$.

tween 1 and 10 s, with the lower bound remained the same as that in the central region. The upper bound of the scaling range is reduced by a factor of 2 when compared with that at the cell center because the large-scale fluctuations are cut off by the nearby cell wall. Similarly, good power-law scaling is also found for the two horizontal moments $\langle(\epsilon_\tau^x)^p\rangle/(\epsilon_0^x)^p$ and $\langle(\epsilon_\tau^y)^p\rangle/(\epsilon_0^y)^p$ (not shown). Using a fixed scaling region in τ (which is chosen from the $p=6$ curve), we fit all the data to a power law and find the exponents $\mu^i(p)$ $(i=x,y,z)$ for all values of p up to 6.

Figure 12 compares the three power-law exponents $\mu^x(p)$ (circles), $\mu^y(p)$ (triangles), and $\mu^z(p)$ (diamonds) as a function of p. The scaling exponents in the two horizontal directions overlap very well and can be described by the same equation as observed at the cell center [Eq. (8)] and with the same set of parameters c, λ and β, given in Eq. (14) (dashed line). Figure 12 thus demonstrates that the horizontal exponents $\mu^i(p)$ $(i=x,y)$ near the sidewall remain the same as those at the cell center. The vertical exponent $\mu^z(p)$ is, however, different from the horizontal exponents and can be described by Eq. (8) with a different set of parameters c, λ, and β given below (solid line)

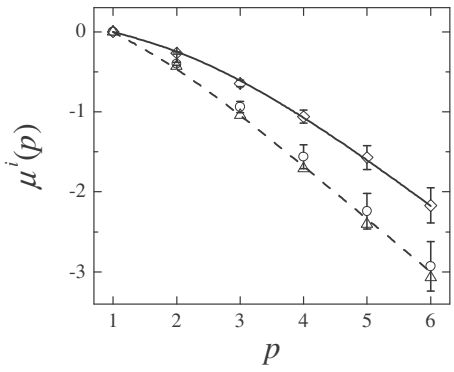

FIG. 12. Measured power-law exponents $\mu^x(p)$ (circles), $\mu^y(p)$ (triangles), and $\mu^z(p)$ (diamonds) as a function of p near the sidewall at $\mathrm{Ra}=8.3\times10^9$. Error bars are shown for circles and diamonds. The dashed line is a plot of Eq. (8) with $c=1$, $\lambda=2/3$, and $\beta=1/3$ [Eq. (14)]. The solid line is a plot of Eq. (8) with $c=2$, $\lambda=2/3$, and $\beta=2/3$ [Eq. (15)].

$$c=2, \quad \lambda=\tfrac{2}{3}, \quad \beta=\tfrac{2}{3}. \tag{15}$$

(Vertical exponent in sidewall region).

As discussed in Sec. II, the value of λ is determined by the strength of buoyancy effects, which should only depend on the height of the measuring position. This is indeed observed with the value of λ $(=2/3)$ obtained in the sidewall region (at midheight of the cell) remaining the same as that at the cell center. On the other hand, the value of c changes with the orientation with the vertical exponent being different from the horizontal ones. For the vertical exponent near the sidewall, we find $c=2$, suggesting that the most dissipative structures along the vertical direction are filamentlike.

C. Near the lower conducting plate

Unlike the situation in the bulk and sidewall regions, temperature fluctuations near the lower conducting plate are governed by a characteristic length, i.e., the thermal boundary layer thickness δ, which decreases with increasing Ra.[58,61] Figure 13 shows the measured mean temperature profile $T(z)$ (open circles) and rms temperature profile $\sigma_T(z)$ (solid circles) as a function of the vertical distance z away from the center of the bottom plate. The measurements are made by moving the temperature probe vertically along the central axis of the cell at a fixed $\mathrm{Ra}=1.75\times10^9$. In the plot, the mean temperature $T_{\mathrm{bot}}-T(z)$ relative to the bottom plate temperature T_{bot} is normalized by $\Delta T/2$ and $\sigma_T(z)$ is normalized by ΔT. The vertical distance z is normalized by δ [$\simeq0.99$ mm at $\mathrm{Ra}=1.75\times10^9$ (Ref. 61)]. It is seen that the measured $\sigma_T(z)/\Delta T$ peaks at the shoulder of the thermal boundary layer with $z/\delta\simeq0.55$ (dashed line).

To study the scaling behavior of $\epsilon_\tau(\mathbf{r},t)$ near the lower conducting plate, we examine three sets of time series data. One is obtained at a fixed value of $\mathrm{Ra}(=1.75\times10^9)$ but with varying positions z; at each position we typically take 8-h-long time series data (corresponding to 1.15×10^6 data points). The other two sets of data are obtained at two fixed locations ($z=0.3$ mm and $z=0.9$ mm, respectively) but with varying Ra $(9\times10^8\le\mathrm{Ra}\le9\times10^9)$; at each Ra, we typically take 8-h-long time series data. It is found that the scaling behavior of $\epsilon_\tau(\mathbf{r},t)$ near the thermal boundary layer can be

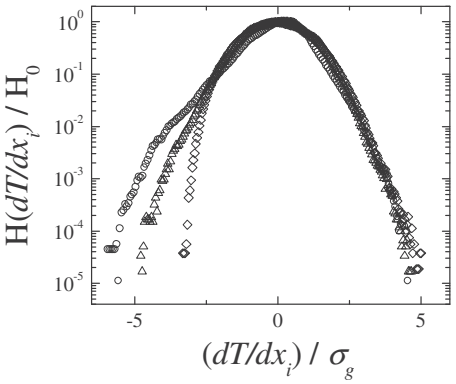

FIG. 14. Measured histograms $H(dT/dx)/H_0$ (circles), $H(dT/dy)/H_0$ (triangles), and $H(dT/dz)/H_0$ (diamonds) for the three components of the temperature gradient vector at $\mathrm{Ra}=1.75\times10^9$. The measurements are made at the vertical distance $z/\delta\simeq0.66$ above the center of the lower conducting plate.

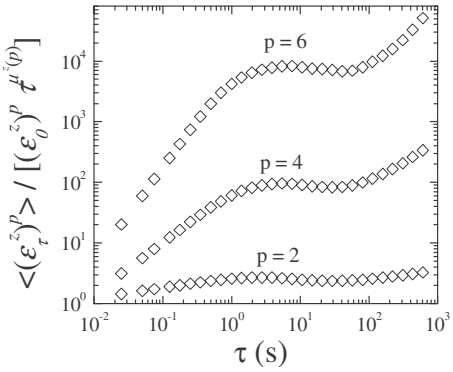

FIG. 15. Compensated plots $\langle(\epsilon_\tau^z)^p\rangle/[\langle(\epsilon_0^z)^p\tau^{\mu^z(p)}]$ as a function of τ for $p=2$, 4, and 6 (from bottom to top). The measurements are made at $z/\delta\simeq0.66$ with $\mathrm{Ra}=1.75\times10^9$.

classified into two distinct regions. (i) Peak region ($0.5\lesssim z/\delta\lesssim0.9$) is located around the peak of the measured $\sigma_T(z)$ (near the dashed line shown in Fig. 13), which is on the verge of the boundary layer and there are many detached thermal plumes in the region. (ii) Outer region ($z/\delta\gtrsim1.05$) is a transition region further away from the boundary layer, where the mean temperature gradient becomes small.

All the time series data obtained at different values of z and Ra can be characterized by the two scaling regions, once they are presented in units of the normalized distance z/δ. In this section, we focus our attention on the scaling behavior of $\epsilon_\tau(\mathbf{r},t)$ in peak region. The transitional behavior of $\epsilon_\tau(\mathbf{r},t)$ in the outer region has been reported elsewhere.[46] Because of the limited resolution of the temperature gradient probe used in the experiment, we were unable to resolve the detailed changes of $\epsilon_\tau(\mathbf{r},t)$ deep inside the thermal boundary layer ($z/\delta\lesssim0.4$), where the mean temperature gradient is large but there are not many detached thermal plumes. The measured histogram of temperature fluctuations in this region is symmetric and has a Gaussian shape.

Figure 14 shows the normalized histograms $H(dT/dx)/H_0$ (circles), $H(dT/dy)/H_0$ (triangles), and $H(dT/dz)/H_0$ (diamonds) for the three components of the temperature gradient vector. To compare the three histograms in the same graph, we normalize the gradient variables dT/dx_i ($x_i=x,y,z$) by their standard deviation σ_g. The measurements are made at $z/\delta\simeq0.66$ above the center of the lower conducting plate. At this location, the LSC is along the x-axis and shears the entire thermal boundary layer. Such a shearing introduces asymmetric fluctuations in the x-z plane, causing the histograms $H(dT/dx)/H_0$ and $H(dT/dz)/H_0$ to be asymmetric. The histogram $H(dT/dy)/H_0$ is more symmetric because the flow along the y-axis perpendicular to the LSC plane is symmetric.

Figure 15 shows the compensated plot of the moments $\langle(\epsilon_\tau^z)^p\rangle/[\langle(\epsilon_0^z)^p\tau^{\mu^z(p)}]$ as a function of τ for $p=2$, 4, and 6 (from bottom to top). Similar to the situation at the cell center and near the sidewall, a common scaling (flat) region in τ is found for every value of p, suggesting that $\langle(\epsilon_\tau^z)^p\rangle$ has a good power-law scaling on τ. The scaling range in τ is between 4 and 21 s, with the upper bound remained the same as that in the central region. The lower bound of the scaling range is increased by a factor of 4 when compared with that at the cell center. In the numerical simulation by Calzavarini *et al.*,[23] the local Bolgiano scale near the bottom plate was found to be $L_B(0)/H\simeq0.1$. The corresponding Bolgiano time is $\tau_B(0)=\tau_0L_B(0)/H\simeq3.5$ s. Thus, the scaling range near the bottom plate starts from $\tau_B(0)$ and ends before the large-scale turnover time τ_0. Similarly good power-law scaling is also found for the two horizontal moments $\langle(\epsilon_\tau^x)^p\rangle/\langle(\epsilon_0^x)^p$ and $\langle(\epsilon_\tau^y)^p\rangle/\langle(\epsilon_0^y)^p$ (not shown).

Figure 16 shows the obtained power-law exponents $\mu^x(p)$ (circles), $\mu^y(p)$ (triangles), and $\mu^z(p)$ (diamonds) as a function of p. The three scaling exponents overlap very well and can be described by Eq. (8) with a common set of parameters c, λ, and β, given below (solid line)

$$c=1,\quad \lambda=\tfrac{2}{5},\quad \beta=\tfrac{3}{5}. \qquad \text{(Inside the thermal boundary layer).} \tag{16}$$

The data can be adequately described by Eqs. (8) and (16) without any adjustable parameter. As discussed in Sec. II, the value $c=1$ suggests that the most dissipative structures inside the thermal boundary layer are sheetlike. In fact, the most

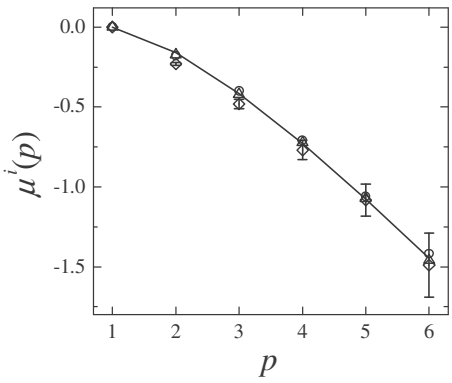

FIG. 16. Obtained power-law exponents $\mu^x(p)$ (circles), $\mu^y(p)$ (triangles), and $\mu^z(p)$ (diamonds) as a function of p. Error bars are shown for diamonds. The measurements are made at $z/\delta\simeq0.66$ with $\mathrm{Ra}=1.75\times10^9$. The solid line is a plot of Eq. (8) with $c=1$, $\lambda=2/5$, and $\beta=3/5$ [Eq. (16)].

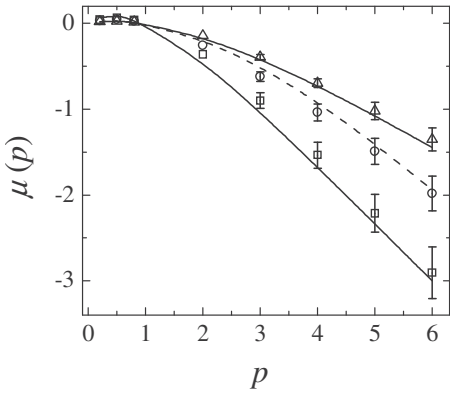

FIG. 17. Power-law exponent of the total dissipation $\mu(p)$ as a function of p obtained at the cell center (squares), near the sidewall (circles), and in peak region inside the lower thermal boundary layer (triangles). Plots of Eq. (8) are shown with three different sets of parameters: (i) $c=1$, $\lambda=2/5$, and $\beta=3/5$ [Eq. (16)] (upper solid line); (ii) $c=2.4$, $\lambda=2/3$, and $\beta=0.72$ (dashed line); and (iii) $c=1$, $\lambda=2/3$, and $\beta=1/3$ [Eq. (14)] (lower solid line). All the measurements are made at $\mathrm{Ra}=8.3\times10^9$.

dissipative structure near the bottom and top plates is the thermal boundary layer itself, which is clearly two-dimensional. The value $\lambda=2/5$ suggests that velocity fluctuations inside the thermal boundary layer obey the Bolgiano–Obukhov scaling[43,44] for buoyancy-dominated flows. This result supports the notion that the largest temperature gradient is concentrated across the thermal boundary layer,[4,9] in which buoyancy effects are strong and temperature becomes an active scalar.

D. Statistics of the total thermal dissipation rate

With the understanding of the scaling behavior of each component of the local thermal dissipation rate, we now discuss the scale-dependent statistics of the total thermal dissipation rate $\epsilon_\tau(\mathbf{r},t)=\Sigma_i\epsilon_\tau^i$. In a recent brief report,[46] we have discussed the scaling behavior of the moments $\epsilon_\tau^p\equiv\langle\epsilon_\tau^p(\mathbf{r},t)\rangle_t$ and showed how the scaling exponent $\mu(p)$, defined by $\epsilon_\tau^p\sim\tau^{\mu(p)}$, changes with varying positions along the central axis of the cylindrical cell from the lower conducting plate to the cell center.

Figure 17 shows the obtained $\mu(p)$ as a function of p at the cell center (squares), near the sidewall (circles), and in peak region inside the lower thermal boundary layer (triangles). As shown in Figs. 6 and 8, the statistics of dissipation fluctuations at the cell center are isotropic and the power-law exponents for each component $\mu^i(p)$ $(i=x,y,z)$ have the same functional form. Similarly, inside the thermal boundary layer, the buoyancy effects are strong and temperature becomes an active scalar. The three individual exponents $\mu^i(p)$ $(i=x,y,z)$, in this case, are also found to have the same functional form, as shown in Fig. 16. As a result, one expects the exponent $\mu(p)$ for the total dissipation rate at the cell center to be well described by the same set of equations [Eqs. (8) and (14)] for passive scalars (lower solid line) and the exponent $\mu(p)$ inside the thermal boundary layer should be well described by the same set of equations [Eqs. (8) and (16)] for active scalars (upper solid line). These results are indeed observed in Fig. 17.

Dissipation fluctuations near the sidewall are found to be anisotropic with the vertical exponent $\mu^z(p)$ having a functional form different from that of $\mu^x(p)$ and $\mu^y(p)$ (see Fig. 12). In this case, one does not expect the total moments $\langle\epsilon_\tau^p\rangle$ to be a simple power law of τ. However, because the contribution from the vertical direction $\epsilon_f^z(\mathbf{r},t)$ near the sidewall is much larger than the horizontal contributions $\epsilon_f^x(\mathbf{r},t)$ and $\epsilon_f^y(\mathbf{r},t)$, we find $\langle\epsilon_\tau^p\rangle$ can still be described by an effective power law and the resulting exponent $\mu(p)$ is adequately described by Eq. (8) with a set of parameters different from those for the individual components. The dashed line in Fig. 17 is a plot of Eq. (8) with $c=2.4$, $\lambda=2/3$, and $\beta=0.72$. Here, the values of c and λ are chosen to best fit the data (circles) whereas β is given by Eq. (11). Clearly, the fitting results for $\mu(p)$ are affected more by the parameters for $\mu^z(p)$ [given in Eq. (15)] than those for $\mu^x(p)$ and $\mu^y(p)$.

It is seen from Fig. 17 that the value of $\mu(p)$ near the sidewall (for a fixed p) is increased when compared with that at the cell center. Using the refined similarity ideas, one finds $\mu(p)$ is directly linked to the scaling exponent $\zeta(p)$ of the temperature structure function $S_p(r)$ [or $S_p(\tau)$]. Thus, the increase in $\mu(p)$ near the sidewall would give rise to an increase in $\zeta(p)$.[42] Indeed, such an increase has been observed in previous measurements of the temperature structure function and power spectrum near the sidewall.[35,38,62] This increase in $\zeta(p)$ was interpreted as a signature for active scalars, but the early interpretations used the global Bolgiano scale L_B (or the corresponding Bolgiano time τ_B) based on the global viscous and thermal dissipation rates averaged over the entire cell. As discussed in Sec. IV A, such an estimate of L_B does not apply to the local regions considered here because of the spatial inhomogeneity of the convective flow in small aspect-ratio cells. Our measurements in Secs. IV B and IV D together clearly demonstrate that the increase in $\mu(p)$ [and hence $\zeta(p)$] is caused by the anisotropy of the flow near the sidewall, so that the codimension of the most dissipative structures is changed from sheetlike to filamentlike, rather than a transition of temperature from being passive to active. This conclusion is further supported by the fact the lower end of the scaling range in τ near the sidewall remains unchanged when compared with that at the cell center.

V. SUMMARY

We have systematically studied the statistical properties of the locally averaged thermal dissipation field in turbulent Rayleigh–Bénard convection. A local temperature gradient probe consisting of four identical thermistors was made to measure the instantaneous thermal dissipation rate $\epsilon_T(\mathbf{r},t)$ in an aspect-ratio-one cell filled with water. The measurements were conducted at a fixed Prandtl number ($\mathrm{Pr}\simeq5.5$) and over varying Rayleigh numbers and spatial positions $\mathbf{r}$ across the convection cell. From the measured $\epsilon_T(\mathbf{r},t)$ we construct a locally averaged thermal dissipation rate $\epsilon_\tau^i(\mathbf{r},t)$ over a time interval τ, as defined in Eq. (7), and study the τ-dependence of the moments, $\langle(\epsilon_\tau^i)^p\rangle$. It is found that $\langle(\epsilon_\tau^i)^p\rangle$ exhibits good scaling in τ $[\langle(\epsilon_\tau^i)^p\rangle\sim\tau^{\mu^i(p)}]$ for all three contributions from the three temperature gradient components $(i=x,y,z)$ and for

all values of p up to 6. This scaling behavior of $\langle(\epsilon_\tau^i)^p\rangle$ is observed at three representative locations in the convection cell: at the cell center, near the side wall, and near the lower conducting plate.

In the central region of the cell, we find that the scale-dependent statistics of dissipation fluctuations are isotropic and the power-law exponents $\mu^i(p)$ $(i=x,y,z)$ have the same functional form, which is well described by Eq. (8) with the parameters c, λ, and β given in Eq. (14). Furthermore, the exponent $\mu(p)$ for the total dissipation is also well described by the same set of equations. From the obtained values of c, λ, and β in Eq. (14), we conclude that in the central region, the most dissipative structures are sheetlike and temperature behaves like a passive scalar.

Near the lower conducting plate, the large-scale circulation shears the entire thermal boundary layer, which introduces asymmetric dissipation fluctuations in the x-direction (along the large-scale flow) and z-direction (parallel to gravity). Such a shearing, however, only affects the amplitude of dissipation fluctuations and the three power-law exponents $\mu^i(p)$ $(i=x,y,z)$ remain the same. The three exponents can all be described by Eq. (8) with a common set of parameters c, λ, and β, given in Eq. (16). In addition, the exponent $\mu(p)$ for the total dissipation is also well described by the same set of equations. From the obtained values of c, λ, and β in Eq. (16), we conclude that inside the thermal boundary layer, the most dissipative structures are sheetlike and temperature becomes an active scalar. This result agrees with our notion that the thermal boundary layer itself is two-dimensional and is the most dissipative structure near the conducting plate. Inside the thermal boundary layer, the temperature gradient takes the largest value so that temperature is expected to be an active scalar.

In the sidewall region, the velocity field is anisotropic with a dominant mean flow in the vertical (z-) direction. The two horizontal exponents $\mu^i(p)$ $(i=x,y)$ are found to be the same as those at the cell center. The vertical exponent $\mu^z(p)$ is, however, different from those in the horizontal directions and can be described by Eq. (8) with a different set of parameters c, λ, and β, given in Eq. (15). From the obtained values of c, λ, and β in Eq. (15), we conclude that near the sidewall the most dissipative structures are filamentlike and temperature behaves like a passive scalar.

Because of the anisotropy of the flow field near the sidewall, one does not expect the moments $\langle\epsilon_\tau^p\rangle$ for the total thermal dissipation to be a simple power law of τ. However, because the contribution to the local thermal dissipation rate from the vertical direction is much larger than those from the horizontal directions, we find the obtained $\langle\epsilon_\tau^p\rangle$ near the sidewall can still be described by an effective power law and the resulting exponent $\mu(p)$ is adequately described by Eq. (8) with a set of parameters heavily influenced by those for $\mu^z(p)$. It is found that the value of $\mu(p)$ near the sidewall (for a fixed p) is increased when compared with that at the cell center. Our analysis demonstrates that such an increase in $\mu(p)$ (and the observed increase of the scaling exponent for the temperature structure functions) is caused by a change of the codimension of the most dissipative structures from being sheetlike to filamentlike, rather than by a transition of temperature from being passive to active.

Putting these results together, we conclude that the scaling of the thermal dissipation field in turbulent Rayleigh–Bénard convection contains two contributions: a background contribution that comes from the two horizontal exponents $\mu^i(p)$ $(i=x,y)$, which have the same features, and a component from the vertical exponent $\mu^z(p)$. The background contribution has the same value in the bulk region of the cell (including both the central and sidewall regions) with the parameters $c=1$ (sheetlike) and $\lambda=2/3$ (passive scalar) but becomes $c=1$ (sheetlike) and $\lambda=2/5$ (active scalar) in the thermal boundary layer. Superimposed on this background is the contribution from the vertical exponent $\mu^z(p)$, which varies with the position. At the cell center, $\mu^z(p)$ remains approximately the same as the two horizontal exponents, whereas near the sidewall, $\mu^z(p)$ becomes different from $\mu^x(p)$ and $\mu^y(p)$ with the parameters $c=2$ (filamentlike) and $\lambda=2/3$ (passive scalar). Inside the thermal boundary layer, all three exponents $\mu^i(p)$ $(i=x,y,z)$ become identical again but with a different set of parameters $c=1$ (sheetlike) and $\lambda=2/5$ (active scalar).

Our experiment clearly demonstrates that the thermal dissipation field in turbulent convection indeed has the scale-dependent statistics and its scaling in τ is well described by a set of scaling parameters. Such a set of parameters provides a scaling description of flow characteristics, including passive and active temperature fluctuations and geometric shape of the most dissipative structures. The intermittency problem of passive scalars has been studied and understood[63] in the Kraichnan model.[64–66] However, a quantitative experimental study of the correlation between the scaling exponents for the dissipation fluctuations and those for the temperature (passive or active) and velocity structure functions remains to be done. Evidently, the present work represents an important first step toward this direction, particularly in the context of turbulent thermal convection.

ACKNOWLEDGMENTS

This work was supported by the Hong Kong Research Grants Council under Grant Nos. HKUST-603208 (PT) and CUHK-400708 (ESCC).

[1] E. Siggia, "High Rayleigh number convection," Annu. Rev. Fluid Mech. **26**, 137 (1994).
[2] S. Grossmann and D. Lohse, "Scaling in thermal convection: A unifying theory," J. Fluid Mech. **407**, 27 (2000).
[3] S. Grossmann and D. Lohse, "Fluctuations in turbulent Rayleigh Bénard convection: The role of plumes," Phys. Fluids **16**, 4462 (2004).
[4] X.-Z. He and P. Tong, "Measurements of the thermal dissipation field in turbulent Rayleigh-Bénard convection," Phys. Rev. E **79**, 026306 (2009).
[5] A. N. Kolmogorov, "The local structure of turbulence in incompressible viscous fluid for very large Reynolds number," Dokl. Akad. Nauk SSSR **30**, 9 (1941); Proc. R. Soc. London, Ser. A **434**, 9 (1991).
[6] U. Frisch, *Turbulence: The Legacy of A. N. Kolmogorov* (Cambridge University Press, Cambridge, UK, 1995).
[7] A. N. Kolmogorov, "A refinement of previous hypotheses concerning the local structure of turbulence in a viscous incompressible fluid at high Reynolds number," J. Fluid Mech. **13**, 82 (1962).
[8] R. H. Kraichnan, "On Kolmogorov's inertial-range theories," J. Fluid Mech. **62**, 305 (1974).

[9]D. Lohse and K.-Q. Xia, "Small-scale properties of turbulent Rayleigh-Bénard convection," Annu. Rev. Fluid Mech. **42**, 335 (2010).
[10]V. S. L'vov, "Spectra of velocity and temperature fluctuations with constant entropy flux of fully developed free-convective turbulence," Phys. Rev. Lett. **67**, 687 (1991).
[11]E. S. C. Ching and K. L. Chau, "Conditional statistics of temperature fluctuations in turbulent convection," Phys. Rev. E **63**, 047303 (2001).
[12]E. S. C. Ching, "Scaling laws in the central region of confined turbulent thermal convection," Phys. Rev. E **75**, 056302 (2007).
[13]E. S. C. Ching and W. C. Cheng, "Anomalous scaling and refined similarity of an active scalar in a shell model of homogeneous turbulent convection," Phys. Rev. E **77**, 015303(R) (2008).
[14]Z.-S. She and E. Leveque, "Universal scaling laws in fully developed turbulence," Phys. Rev. Lett. **72**, 336 (1994).
[15]E. S. C. Ching and C. Y. Kwok, "Statistics of local temperature dissipation in high Rayleigh number convection," Phys. Rev. E **62**, R7587 (2000).
[16]I. Procaccia and R. Zeitak, "Scaling exponents in nonisotropic convective turbulence," Phys. Rev. Lett. **62**, 2128 (1989).
[17]I. Procaccia and R. Zeitak, "Scaling exponents in thermally driven turbulence," Phys. Rev. A **42**, 821 (1990).
[18]K. R. Sreenivasan, "On local isotropy of passive scalars in turbulent shear flows," Proc. R. Soc. London, Ser. A **434**, 165 (1991).
[19]S. Grossmann and D. Lohse, "Scaling in hard turbulent Rayleigh-Bénard flow," Phys. Rev. A **46**, 903 (1992).
[20]S. Grossmann and D. Lohse, "Characteristic scales in Rayleigh-Bénard turbulence," Phys. Lett. A **173**, 58 (1993).
[21]R. Benzi, S. Ciliberto, R. Tripiccione, C. Baudet, F. Massaioli, and S. Succi, "Extended self-similarity in turbulent flows," Phys. Rev. E **48**, R29 (1993).
[22]R. Kerr, "Rayleigh number scaling in numerical convection," J. Fluid Mech. **310**, 139 (1996).
[23]E. Calzavarini, F. Toschi, and R. Tripiccione, "Evidences of Bolgiano-Obhukhov scaling in three-dimensional Rayleigh-Bénard convection," Phys. Rev. E **66**, 016304 (2002).
[24]R. Camussi and R. Verzicco, "Temporal statistics in high Rayleigh number convective turbulence," Eur. J. Mech. B/Fluids **23**, 427 (2004).
[25]E. S. C. Ching, H. Guo, and W. C. Cheng, "Understanding the different scaling behavior in various shell models proposed for turbulent thermal convection," Physica D **237**, 2009 (2008).
[26]E. S. C. Ching, H. Guo, and T. S. Lo, "Refined similarity hypotheses in shell models of homogeneous turbulence and turbulent convection," Phys. Rev. E **78**, 026303 (2008).
[27]X.-Z. Wu, L. P. Kadanoff, A. Libchaber, and M. Sano, "Frequency power spectrum of temperature fluctuations in free convection," Phys. Rev. Lett. **64**, 2140 (1990).
[28]I. Procaccia, E. S. C. Ching, P. Constantin, L. P. Kadanoff, A. Libchaber, and X.-Z. Wu, "Transitions in convective turbulence: The role of thermal plumes," Phys. Rev. A **44**, 8091 (1991).
[29]P. Tong and Y. Shen, "Relative velocity fluctuations in turbulent Rayleigh-Bénard convection," Phys. Rev. Lett. **69**, 2066 (1992).
[30]R. Benzi, R. Tripiccione, F. Massaioli, S. Succi, and S. Ciliberto, "On the scaling of the velocity and temperature structure functions in Rayleigh-Bénard convection," Europhys. Lett. **25**, 341 (1994).
[31]S. Cioni, S. Ciliberto, and J. Sommeria, "Temperature structure functions in turbulent convection at low Prandtl number," Europhys. Lett. **32**, 413 (1995).
[32]T. Takeshita, T. Segawa, J. A. Glazier, and M. Sano, "Thermal turbulence in mercury," Phys. Rev. Lett. **76**, 1465 (1996).
[33]S. Ashkenazi and V. Steinberg, "Spectra and statistics of velocity and temperature fluctuations in turbulent convection," Phys. Rev. Lett. **83**, 4760 (1999).
[34]S.-Q. Zhou and K.-Q. Xia, "Scaling properties of the temperature field in convective turbulence," Phys. Rev. Lett. **87**, 064501 (2001).
[35]L. Skrbek, J. J. Niemela, K. R. Sreenivasan, and R. J. Donnelly, "Temperature structure functions in the Bolgiano regime of thermal convection," Phys. Rev. E **66**, 036303 (2002).
[36]T. Mashiko, Y. Tsuji, T. Mizuno, and M. Sano, "Instantaneous measurement of velocity fields in developed thermal turbulence in mercury," Phys. Rev. E **69**, 036306 (2004).
[37]G. I. Taylor, "The spectrum of turbulence," Proc. R. Soc. London, Ser. A **164**, 476 (1938).
[38]C. Sun, Q. Zhou, and K.-Q. Xia, "Cascades of velocity and temperature fluctuations in buoyancy-driven thermal turbulence," Phys. Rev. Lett. **97**, 144504 (2006).
[39]R. J. P. Kunnen, H. J. H. Clercx, B. J. Geurts, L. J. A. Bokhoven, R. A. D. Akkermans, and R. Verzicco, "Numerical and experimental investigation of structure-function scaling in turbulent Rayleigh-Bénard convection," Phys. Rev. E **77**, 016302 (2008).
[40]A. M. Obukhov, "Structure of the temperature field in turbulent flow," Izv. Akad. Nauk SSSR, Ser. Geogr. Geofiz. **13**, 58 (1949).
[41]S. Corrsin, "On the spectrum of isotropic temperature fluctuations in isotropic turbulence," J. Appl. Phys. **22**, 469 (1951).
[42]G. Ruiz-Chavarria, C. Baudet, and S. Ciliberto, "Scaling laws and dissipation scale of a passive scalar in fully developed turbulence," Physica D **99**, 369 (1996).
[43]R. Bolgiano, "Turbulent spectra in a stably stratified atmosphere," J. Geophys. Res. **64**, 2226, doi:10.1029/JZ064i012p02226 (1959).
[44]A. M. Obukhov, "The influence of Archimedes forces on the structure of the temperature field in a turbulent flow," Dokl. Akad. Nauk SSSR **125**, 1246 (1959).
[45]A. S. Monin and A. M. Yaglom, *Statistical Fluid Mechanics* (MIT Press, Cambridge, MA, 1975).
[46]X.-Z. He, P. Tong, and E. S. C. Ching, "Statistics of the locally-averaged thermal dissipation rate in turbulent Rayleigh-Bénard convection," J. Turbul. **11**, N35 (2010).
[47]X.-L. Qiu and P. Tong, "Large-scale velocity structures in turbulent thermal convection," Phys. Rev. E **64**, 036304 (2001).
[48]H.-D. Xi, S. Lam, and K.-Q. Xia, "From laminar plumes to organized flows: The onset of large-scale circulation in turbulent thermal convection," J. Fluid Mech. **503**, 47 (2004).
[49]X.-L. Qiu and P. Tong, "Temperature oscillations in turbulent Rayleigh-Bénard convection," Phys. Rev. E **66**, 026308 (2002).
[50]X.-D. Shang, X.-L. Qiu, P. Tong, and K.-Q. Xia, "Measured local heat transport in turbulent Rayleigh-Bénard convection," Phys. Rev. Lett. **90**, 074501 (2003); "Measurements of the local convective heat flux in turbulent Rayleigh-Bénard convection," Phys. Rev. E **70**, 026308 (2004).
[51]A. S. Gurvich and A. M. Yaglom, "Breakdown of eddies and probability distribution for small-scale turbulence," Phys. Fluids **10**, S59 (1967).
[52]B. Dubrulle, "Intermittency in fully developed turbulence: Log-Poisson statistics and generalized scale covariance," Phys. Rev. Lett. **73**, 959 (1994).
[53]Z.-S. She and E. C. Waymire, "Quantized energy cascade and Log-Poisson statistics in fully developed turbulence," Phys. Rev. Lett. **74**, 262 (1995).
[54]M. S. Emran and J. Schumacher, "Fine-scale statistics of temperature and its derivatives in convective turbulence," J. Fluid Mech. **611**, 13 (2008).
[55]X.-L. Qiu and P. Tong, "Onset of coherent oscillations in turbulent Rayleigh-Bénard convection," Phys. Rev. Lett. **87**, 094501 (2001).
[56]E. S. C. Ching, C. K. Leung, X.-L. Qiu, and P. Tong, "Intermittency of velocity fluctuations in turbulent thermal convection," Phys. Rev. E **68**, 026307 (2003).
[57]R. Benzi, F. Toschi, and R. Tripiccione, "On the heat transfer in Rayleigh-Bénard systems," J. Stat. Phys. **93**, 901 (1998).
[58]Y.-B. Du and P. Tong, "Turbulent thermal convection in a cell with ordered rough boundaries," J. Fluid Mech. **407**, 57 (2000).
[59]E. S. C. Ching, "Intermittency of temperature field in turbulent convection," Phys. Rev. E **61**, R33 (2000).
[60]X.-Z. He, P. Tong, and K.-Q. Xia, "Measured thermal dissipation field in turbulent Rayleigh-Bénard convection," Phys. Rev. Lett. **98**, 144501 (2007).
[61]S.-L. Lui and K.-Q. Xia, "Spatial structure of the thermal boundary layer in turbulent convection," Phys. Rev. E **57**, 5494 (1998).
[62]M. Sano, X.-Z. Wu, and A. Libchaber, "Turbulence in helium-gas free convection," Phys. Rev. A **40**, 6421 (1989).
[63]B. I. Shraiman and E. D. Siggia, "Scalar turbulence," Nature (London) **405**, 639 (2000) (and references therein).
[64]R. H. Kraichnan, "Small-scale structure of a scalar field convected by turbulence," Phys. Fluids **11**, 945 (1968).
[65]R. H. Kraichnan, "Convection of a passive scalar by a quasi-uniform random straining field," J. Fluid Mech. **64**, 737 (1974).
[66]R. H. Kraichnan, "Anomalous scaling of a randomly advected passive scalar," Phys. Rev. Lett. **72**, 1016 (1994).